# WHY DO DISILANES FAIL TO FLUORESCE?

Matthew K. MacLeod[a1] and Josef Michl[a2,b,*]

[a] *Department of Chemistry and Biochemistry, University of Colorado, Boulder, Colorado 80309, USA; e-mail:* [1] *macleod@eefus.colorado.edu,* [2] *michl@eefus.colorado.edu*

[b] *Institute of Organic Chemistry and Biochemistry, Academy of Sciences of the Czech Republic, v.v.i., Flemingovo nám., 2, 166 10 Prague 6, Czech Republic*

Received October 27, 2011
Accepted October 30, 2011
Published online February 3, 2012

*Dedicated to Dr. Zdeněk Havlas on the occasion of his 60th birthday.*

In contrast to longer peralkylated oligosilanes, many of which fluoresce efficiently, disilanes and trisilanes exhibit no detectable fluorescence even at low temperatures. This is especially striking in the case of disilanes, whose $S_1$-$S_0$ transition is quite strongly allowed, and which must have very efficient electronic excited state deactivation mechanisms. To identify them, we examine the lowest excited singlet state potential energy surface $S_1$ of $Si_2Me_6$ with TDDFT (B3LYP/TZVP, PBE0/TZVP and BHLYP/TZVP) and ab initio (RICC2/TZVP and RIADC(2)/TZVP) methods and identify several shallow minima and nearby funnels. Relaxed excited state structures show strong valence rehybridization relative to the ground state, allowing optimal accomodation of the simultaneous presence of a negative and a positive charge in their Lewis structures. Efficient decay pathways and relations to longer oligosilanes are discussed.

**Keywords**: Excited states; Relaxed excited state; Excited state potential energy minima; Rydberg; Conical intersection; Funnel; Molecular orbitals; Artificial charge transfer; Disilane; Hypervalent Si; Excitation localization; TDDFT; RICC2; RIADC(2).

## INTRODUCTION

### *Electronic Excitation in Saturated Molecules*

Saturated molecules such as the oligosilanes contain only single bonds and possibly lone pairs, and the study of their photophysics is generally difficult. Their excitation energies are usually high and electronically excited states tend to be packed closely together, making both calculations and experiments harder. Because there often is no secondary means of holding the termini of a single bond together, as there is in multiple bonds, local-



doi:10.1135/cccc2011179

ized σσ* excitation of a bond in a saturated system has the potential for destroying the link between the termini completely and causing a fast and profound modification of the molecular geometry.

At first sight, any localized σσ* excitation of a single bond would appear to be always dissociative, since an electron in a σ orbital is less bonding than an electron in a σ* orbital is antibonding. However, this argument holds only for the triplet. More detailed consideration of allowed singlet σσ* excitation[1] shows that it will be dissociative only if the resulting biradical is tritopic[2] or of even higher topicity, or if the two termini have very different electronegativities. If the electronegativities are equal or similar, e.g., in the simplest case of $H_2$, the $S_1$ excited state can be thought of as a zwitterionic tight ion pair[1,3], possibly with Rydberg character. Such an excited singlet is bound with respect to bond stretching, since charge separation costs energy. In polyatomic molecules deep-seated structural changes are still likely, but instead of merely stretching one bond as in the triplet, the lowest singlet excited molecule may often find an energetically better way in which a large geometrical distortion either accommodates the simultaneous presence of a positive and a negative charge in a zwitterionic valence bond structure, or induces a transformation to a covalent excited singlet state, often by proceeding to a region of a conical intersection.

These significant geometrical changes and the associated large stabilization energies normally cause singlet excitation in a saturated molecule to localize. Even if a structural motif such as a C–C bond is repeated several times, offering an opportunity for a significant energy saving by conjugation if a strong geometrical distortion were avoided, this saving would rarely exceed that achieved by an excitation localizing geometrical distortion (in the language of solid state physics, the exciton band half-width in the extended system of excitation sites is almost always smaller than the site distortion energy). Along the way from a starting vertical geometry reached upon an $S_0$ to $S_1$ excitation to a distant strongly non-vertical minimum in the $S_1$ surface a conical intersection is likely to be encountered, causing decay to the ground state. Fluorescence from $S_1$ to $S_0$ is absent or weak, and if observed at all, it is strongly Stokes-shifted[4].

Against this general backdrop, a fairly unique and well recognized class of saturated compounds that can be exceptionally strongly fluorescent with minimal Stokes shift are the all-transoid[5] conformers of long peralkylated polysilanes $Si_nR_{2n+2}$ (R = alkyl)[6]. When $n > 6$, the stabilization of $S_1$ by conjugation exceeds the site distortion energy, making excitation localizing strong geometrical distortions unfavorable[7]. In a very long chain the exciton stretches over 20–30 Si–Si bonds[8]. These saturated compounds thus

carry strongly delocalized $S_1$ excited states and in many respects resemble conjugated π-electron compounds[6]. In contrast, when $n < 7$, or if the conformation is not close to all-transoid[9,10], the stabilization of $S_1$ in an all-transoid conformer by conjugation at near vertical geometry is insufficient (cf. quantum confinement), and distortion to a localized excited state takes place. Such short oligosilanes thus behave like most ordinary saturated compounds, but their excitations are easier to study than those of the otherwise isostructural alkanes, because they occur at lower energies. It has been proposed[11] that the difference in excitation energies can be traced back to the lower electronegativity of silicon relative to carbon.

Our current interest is the nature of the geometrical distortions that localize the electronic excitation in the $S_1$ state of all-transoid $Si_nR_{2n+2}$ with $n < 7$ and of most other confomers for any $n$. The first absorption peak of these oligosilanes still follows the trend set by the longer members of the series and blue shifts as the chain is shortened, in quantitative agreement with TDDFT B3LYP/TZ calculated vertical excitation energies[12]. However, no fluorescence from a delocalized state is observed, and similarly as certain alkanes and cycloalkanes[4], these oligosilanes emit a very broad hugely Stokes-shifted band. Some conformers fluoresce in the blue[7,13] (26–30 000 $cm^{-1}$) and others in the green[14,15] (~20 000 $cm^{-1}$). The quantum yield of these emissions drops with increasing temperature and with decreasing chain length. Octamethyltrisilane and hexamethyldisilane do not emit measurably even at 14 K [16]. The nature of the excited state geometry is not known either for the blue or for the green fluorophore, but it has been suggested that the blue emission originates at a geometry in which one Si–Si bond has been stretched[17,18].

Some hints as to the nature of the conical intersections responsible for the prevalent $S_1$-$S_0$ radiationless decay are offered by observations of photochemical products[6,19]. (i) In a chain abridgement process, a dialkylsilylene is extruded, a new Si–Si bond is formed, and the silicon backbone is shortened by one Si atom. The silylene can be trapped[20] or observed directly[21,22]. The conical intersection responsible for this process has been identified computationally[23,24]. This is often the dominant process, but is only possible in trisilanes and longer chains. (ii) In another reductive elimination, a silylsilylene is extruded and a new Si–C bond is formed. A subsequent ground-state rearrangement of the silylsilylene to a disilene is followed by further thermal reactions[25]. (iii) In a third process, homolytic cleavage of a Si–Si bond takes place. The formation of two radicals has been attributed to a reaction in a $T_1$ state reached from $S_1$ by intersystem crossing[23] but it has also been proposed[24] that it is one of the outcomes to be expected

for decay through the above conical intersection (i) that leads to a dialkylsilylene.

*Molecular Orbitals and Excited States in Saturated Systems*

Although all valence excitation in saturated systems without lone pairs, such as the oligosilanes, necessarily is from bonding orbitals of σ type to antibonding orbitals of σ* type, it is useful to distinguish two types of delocalized molecular orbitals (MOs) in an oligosilane chain[6,10]. Those that are symmetric with respect to the local Si–Si–Si plane are said to be of local σ character and those that are locally antisymmetric, of local π character. The overall character is obtained by averaging over all Si atoms, weighted by the amplitudes of the orbital on each. In oligosilanes with a planar Si backbone, an MO must be of either pure σ or pure π character. At more general geometries, the local characters and the overall characters are intermediate between pure σ and pure π, and could be labeled as mixed (μ), but very often an MO can still be classified as primarily σ or primarily π in nature.

Low-energy vertical excitations in linear oligosilanes are now quite well understood[6,9,12,14]. All are due to promotions of electrons from occupied Si–Si bonding MOs that are purely or almost purely σ in character, particularly from the least bonding among them, the HOMO. This MO has no nodal planes across Si–Si bonds and a nodal surface going through each Si atom. In an infinite chain, it can be viewed as a combination of $3p_x$ atomic orbitals from all Si atoms (the *x* axis lies in the chain direction, the *y* axis is in the local Si–Si–Si symmetry plane, and the *z* axis is perpendicular to this plane). The excitations lead to two types of valence excited states, σσ* and σπ*, depending on the nature of the terminating MO. In oligosilanes with a non-planar skeleton of silicon atoms excited states of strongly mixed nature are also possible but are relatively rare. This is especially true in the all-transoid conformers, whose silicon skeleton is almost planar and the σσ*, σπ* nomenclature quite satisfactory[10]. The lowest σ* and π* MOs in peralkylated oligosilanes are of comparable energy and one or the other is the lowest unoccupied molecular orbital (LUMO). The σ* MOs are composed of Si–Si antibonding orbitals and the π* MOs are composed of Si–C antibonding orbitals. Because of the electronegativity difference between Si and C, the latter antibonding orbitals have a larger amplitude on the Si than the C atom. The lowest energy σ* MO of the infinite chain has a node across every Si–Si bond and an antinode at each Si atom, and can be viewed

as a combination of 3s with some $3p_y$ Si atomic orbital contributions from each Si atom. Low energy π* orbitals can be viewed as combinations of $3p_z$ Si atomic orbitals, with smaller contributions on the alkyl substituents. In an infinite chain, the most stable among them has no nodes across Si–Si bonds, and an excitation from the HOMO into it is forbidden by the local symmetry at each Si atom. In chains of finite length, chain-end effects cause minor modifications, but the first σσ* transition remains strongly allowed and the first σπ* transition extremely weak, except in disilane, where it is strong, since in this case the nodal properties of the σ and the π* MOs match[26,27].

As the polysilane chain is shortened, the energy of the lowest σ* MO increases faster than that of the lowest π* MO. In the permethylated series, the first σσ* and the first σπ* vertical excited singlets are approximately degenerate in tetrasilane. In the longer chains, the first vertical excited state is of σσ* nature, and in the shorter chains, it is of σπ* nature. In hexamethyldisilane (**1**), the two states differ considerably in their energies[26,27]. The first vertical σπ* state occurs at ~52 000 $cm^{-1}$ and states of σσ* nature are believed to be located above 62 000 $cm^{-1}$. The energies of the σπ* and σσ* states are reduced at different rates when the Si–Si bond is stretched, and in hexa-*tert*-butyldisilane the lowest σσ* absorption peaks at 51 500 $cm^{-1}$ and its 0-0 component lies below that of the σπ* transition[27].

*The Present Objective*

In view of the above discussion, the absence of all fluorescence in disilanes and trisilanes might appear unexceptional, since after all, they are fully saturated compounds. Yet, given that most if not all longer oligosilanes fluoresce, even though some only weakly, it is puzzling. It is tempting to attribute the absence of fluorescence in trisilanes to the circumstance that the formally forbidden σπ* state is now the lowest, but this argument cannot be made for disilane, where the transition to a σπ* state is quite strongly allowed. It appears that in both compounds conical intersections are encountered along the way to a strongly distorted minimum and bring about a rapid decay to $S_0$. It has been proposed that the return through a conical intersection leading to the extrusion of a silylene is responsible for the absence of fluorescence from a trisilane[23,24], and that the situation in tetrasilane is similar[28], but the nature of the conical intersection responsible for the decay of $S_1$ of the disilane **1** remains unknown and it is the subject of the present investigation. It is hoped that the patterns of excita-

tion localization and return to $S_0$ found in hexamethyldisilane will likely be applicable also in longer oligosilanes, where these processes are less dominant.

A complete search of the $S_1$ surface of **1** is precluded by the number of atoms present in the molecule, and we have focused our general search for excited state minima and regions of near $S_0$-$S_1$ degeneracy (funnels) to regions of geometries that are relatively close to the ground state equilibrium geometry. After an initial vertical excitation, they are likely to be reached first, and if they return the molecule to the $S_0$ state, the presence of additional more distant funnels will be irrelevant. We have looked for stationary points and used vibrational frequency analysis to distinguish between minima and saddle-points. When the optimization led to a region of very small $S_1$-$S_0$ energy differences, we assumed that a funnel was present. We made no attempts to determine whether the funnels corresponded to true conical intersections or to regions of nearly avoided surface touching, and did not try to pinpoint the exact location of the conical intersections possibly present. The single-reference methods of calculation available for molecules of this size are not appropriate for regions of near degeneracy, and these distinctions have no practical consequences for our purposes. Once the energy difference between $S_1$ and $S_0$ is less than a few thousand $cm^{-1}$, return from $S_1$ to $S_0$ becomes so fast that further travel on the $S_1$ surface becomes very unlikely in any event. The difference between near degeneracy and exact degeneracy between $S_1$ and $S_0$, as well as the exact location of the minimum energy in the conical intersection subspace then become immaterial[3].

## COMPUTATIONAL METHODS

Ground state geometry optimizations for hexamethyldisilane were carried out with the B3LYP[29], PBE0[30,31] and BHLYP[32] functionals with the TZVP[33], and aug-cc-pVDZ[34] basis sets, using Turbomole 6.2[35]. Ab initio optimizations with the approximate singles and doubles coupled-cluster (RICC2)[36] and the polarization propagator RIADC(2) method (algebraic diagrammatic construction through second order)[37] and TZVP basis sets were also carried out. These ground state optimizations were used to obtain starting structures for excited state optimization as well as structures needed to obtain Stokes shifts and site distortion energies. The geometry of the radical cation of hexamethyldisilane was optimized with the RIUMP2/def2-TZVP method[38] as implemented in Turbomole. Throughout this work, the B3LYP functional used was the version which employs the VWN 5 correlation

functional[39]. For DFT calculations large integration grids (size 5)[40] were used.

$S_1$ geometry optimizations were done both with time-dependent density functional theory[41] (TDDFT) in the Tamm–Dancoff approximation (TDA) with various functionals (B3LYP, PBE0, BHLYP), and with the ab initio methods listed above, using the Ahlrichs TZVP basis set on all atoms and Turbomole 6.2 [42,43]. Excited state convergence criteria were set to gradient differences of $1 \times 10^{-6}$ and energy differences of $1 \times 10^{-9}$ Hartree. Excited state vibrational analysis was used to identify minima.

Vertical excitation (emission) energies at each relaxed $S_1$ stationary point were calculated with TDDFT in the random phase approximation (RPA) and the B3LYP functional and def2-TZVP basis set in Turbomole 6.2. Oscillator strengths were obtained with the length description of the transition dipole moment operator. The site distortion energy was then computed as the difference between the vertical Franck–Condon and relaxed $S_1$ energies, and the Stokes shift was obtained as the difference between the vertical absorption and emission electronic energies.

Due to diffuse nature of the first excited state of some $S_1$ minima, the aug-cc-pVDZ basis set was also used with the B3LYP functional. Functionals that are not asymptotically corrected are known to underestimate excitation energies for charge transfer and Rydberg states and this approximation was therefore checked by additional calculations involving various asymptotically corrected functionals (the CAM-B3LYP [44] and LC-BLYP [45] functionals from GAMESS [46], October 1, 2010 version), as well as with the RICC2 ab initio method to calculate excitation energies. The range correction cutoff parameter μ was optimized to a value of 0.23 $a_0^{-1}$ that reproduces the σπ* experimental excitation energy of disilane (denoted as the LC′-BLYP method). Minimal augmentation was also added to basis sets in the style of the maug-cc-pVTZ basis set[47]. The def2-TZVP-mD basis set refers to a similarly minimally augmented basis set where an additional diffuse s function was added to the Si, C and H def2-TZVP basis sets. The exponents for these functions were taken from the def2-TZVP-D basis set[48] in the case of Si and C and from the aug-cc-pVTZ basis set[49] for H.

An excited state stochastic search for local minima was run on **1** with TDDFT. To do this, a Fortran 90 program was written to apply random stochastic displacements to the nuclei, followed by excited state optimization with the PBE0/SVP method, using Turbomole 6.2. Here a set of 100 structures were generated by random kicks limited to 50% of the ground state Si–Si bond distance for Si atoms, 40% of the Si–C ground state bond length for C, and 30% of the C–H ground state bond length for H.

To test the ground state fate of **1** deposited into various funnels, stochastic kicks were applied to the corresponding structures. The size of one set of displacements was limited to 20% of the ground state Si–Si bond distance for Si, 10% of the Si–C ground state bond length for C, and 5% of the C–H ground state bond length for H. In a second set, larger kicks were applied where the maximum displacement sizes were increased by a factor of three. Finally, a set of displacements with increased Si–Me kicks were carried out as some excited state minima and structures in the $S_0$-$S_1$ funnel region had large Si–C bond stretching. The displacements were limited to 50% of the ground state Si–Si bond distance for Si, 50% of the Si–C ground state bond length for C, and 25% of the C–H ground state bond length for H. Approximately 100 optimization paths for each set were run with the CASSCF(8,8)/6-31G* method for each parent structure. In some cases an active space of 10 electrons in 10 orbitals was required for wave function convergence. The CASSCF calculation were employed with the FORS approach in GAMESS.

Natural bond orbital analysis[50] of the configuration interaction singles (CIS) wave function was performed at the CIS/6-311G(d,p) level with the NBO 5.9 [51] program linked to the GAMESS program suite.

## RESULTS

To summarize briefly, four different minima in the $S_1$ surface of hexamethyldisilane (**1a–1d**) have been located by one or more methods of calculation, plus another (**1z**) that could be present in condensed media. At structures **1a–1c**, $S_1$ is a valence state, and at structure **1d**, it is a Rydberg state. Two of the structures, **1a** and **1b**, resemble those that have been recently found responsible for the blue and green emission from somewhat longer oligosilanes, respectively[52]. Various structures near $S_0$-$S_1$ touching (funnels **1α** to **1δ**) and ground state return products have also been identified.

### *Excited State Geometry Relaxation*

Excited state optimization for hexamethyldisilane started at various choices of geometry. (i) One was the ground state $D_{3d}$ equilibrium geometry **1**, at which the lowest observed[26] excited singlet state is of σπ* nature. This is a valence state and is reproduced well by calculations[27], which also predict the presence of an unobserved symmetry-forbidden Rydberg state at lower energies, and additional Rydberg states may be present as well. (ii) Another

was a geometry **1***, similar to that **1**, but with the Si–Si bond stretched to 2.5 Å and the Si(1)–Si(2)–C(1) valence angles increased to 120°. At this geometry, the lowest singlet valence state is calculated to be of σσ* character, and there are experimental indications[26] that the resulting change in the order of the σπ* and σσ* states is indeed correct. (iii) A third choice was a set of geometries **1**** derived from structure **1** by stochastic kicks to Si, C and H. In order to assure that the optimization involves valence states in as much as possible, it was performed without diffuse functions in the basis set. The structures resulting from optimization of the lowest valence excited state of **1**, **1*** and **1**** are shown in Fig. 1. In three of them (**1a**, **1b** and **1c**)

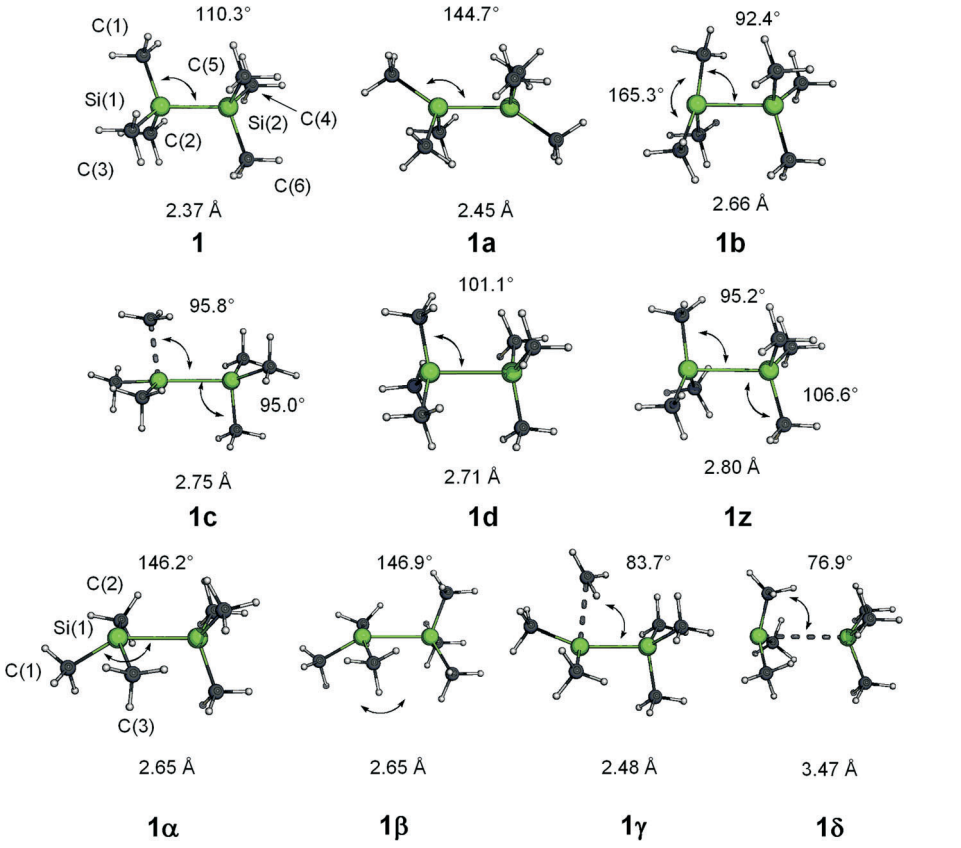


FIG. 1

$S_1$ stationary points (**1a**–**1d**, **1z**) and approximate $S_1$–$S_0$ funnel geometries (**1α**–**1δ**) from calculations using basis sets without diffuse functions, except for **1d**. Si–Si bond lengths in Å and various Si–C–Si or C–Si–C angles (double-headed arrows) in deg. For atom numbering, see **1**

the $S_1$ state is of valence nature, and in one (**1z**) it has some diffuse character. Diffuse functions were then added to the basis set and the structures were subsequently optimized further. The $S_1$ state of structure **1z** acquired Rydberg character in the process and the geometry converged to **1d**, but the nature of the $S_1$ states of **1a**, **1b** and **1c** remained valence.

Starting at the vertical geometry **1**, optimization on the $S_1$ surface without diffuse functions in the basis set resulted in three stationary points (**1a**, **1b**, **1z**) and one funnel, **1α**, depending on the method used. Addition of diffuse functions did not affect **1a** and **1b** significantly, but a B3LYP/aug-cc-pVDZ optimization of both **1** and **1z** gave **1d**. Structures of the stationary points on $S_1$ obtained by different methods were very similar.

Both RIADC(2) and RICC2 with the TZVP basis set produced **1a**, whereas only the TDDFT B3LYP/TZVP and no other method yielded **1z**. $S_1$ optimization of **1z** with the BHLYP/TZP method led to the funnel **1α**. With both the RIADC(2)/TZVP and RICC2/TZVP methods it yielded **1γ** instead. Optimization of **1** with TDDFT PBE0/TZVP led directly to **1b** and with TDDFT BHLYP/TZVP, to the funnel **1α**.

Results obtained starting at the geometry **1*** also depended strongly on the method of calculation used. While all methods led to the stationary point **1a**, only with the PBE0/TZVP method was this a minimum. Other functionals as well as RIADC(2)/TZVP and RICC2/TZVP ab initio methods produced similar stationary structures, but they were saddle-points (transition states). However, since the PBE0/TZVP minimum was extremely shallow, for practical purposes all the methods give the same outcome.

Starting from structures **1****, generated by stochastic search, TDDFT PBE0/TZVP yielded the structures **1a**, **1α** and **1b**, as well as **1c**, which proved to be a minimum on $S_1$ only when reoptimized with the TDDFT B3LYP/TZVP method. Optimization of **1c** with the PBE0/TZVP, BHLYP/TZVP and RICC2/TZVP methods led the molecule to the funnel **1α**, and optimization with RIADC(2)/TZVP method led to a different funnel, **1β**.

*The Blue Structure **1a***

All stationary points obtained for **1a** belong to the $C_i$ symmetry group and its important geometrical parameters are listed in Table I. This structure is referred to as "blue", because its analogs in somewhat longer silanes are believed[52] to be responsible for their reported[7] blue emission. The calculated Si–Si bond lengths range from 2.454 Å (PBE0/TZVP) to 2.560 Å (RIADC(2)/TZVP). The C(1)–Si(1)–Si(2) valence angle is increased from 110.3° in the ground state (PBE0/TZVP) to values from 142.8° (BHLYP/TZVP) to 147.0°

TABLE I
Geometrical parameters for stationary points on the $S_1$ surface of the blue minimum **1a**, optimized with TDDFT PBE0/TZVP (minimum), BHLYP/TZVP, RIADC(2)/TZVP and RICC2/TZVP (transition states)

| Structure | ∠C–Si–C, ° | ∠C–Si–Si, ° | Si–Si, Å | Si–C, Å |
|---|---|---|---|---|
| $Si_2Me_6$ | 110.2 | 89.0 | 2.454 | 1.981 |
| PBE0/TZVP | 103.2 | 102.9 | | 1.904 |
| $C_i$ | 103.6 | 144.7 | | 1.934 |
| **1a** | 110.2 | 89.0 | | 1.981 |
| | 103.2 | 102.9 | | 1.934 |
| | 103.6 | 144.7 | | 1.904 |
| $Si_2Me_6$ | 108.6 | 89.9 | 2.473 | 2.017 |
| B3LYP/TZVP | 102.9 | 104.2 | | 1.913 |
| $C_i$ | 102.4 | 144.7 | | 1.950 |
| **1a** | 108.6 | 89.9 | | 2.017 |
| | 102.9 | 104.2 | | 1.913 |
| | 102.4 | 144.7 | | 1.950 |
| $Si_2Me_6$ | 113.0 | 91.0 | 2.554 | 1.935 |
| BHLYP/TZVP | 104.3 | 99.1 | | 1.903 |
| $C_i$ | 105.6 | 142.8 | | 1.920 |
| **1a** | 113.0 | 91.0 | | 1.935 |
| | 104.3 | 99.1 | | 1.903 |
| | 113.0 | 142.8 | | 1.920 |
| $Si_2Me_6$ | 111.4 | 88.2 | 2.560 | 1.941 |
| RIADC(2)/TZVP | 104.5 | 98.0 | | 1.906 |
| $C_i$ | 105.3 | 147.0 | | 1.924 |
| **1a** | 111.4 | 88.2 | | 1.941 |
| | 104.5 | 98.0 | | 1.906 |
| | 105.3 | 147.0 | | 1.924 |
| $Si_2Me_6$ | 111.4 | 88.3 | 2.541 | 1.946 |
| RICC2/TZVP | 104.3 | 98.6 | | 1.907 |
| $C_i$ | 105.1 | 146.7 | | 1.926 |
| **1a** | 111.4 | 88.3 | | 1.946 |
| | 104.3 | 98.6 | | 1.907 |
| | 105.1 | 146.7 | | 1.926 |

(RIADC(2)/TZVP). The C(2)–Si(1)–Si(2) angle is reduced to values from 88.2° (RIADC(2)/TZVP) to 91.0° (BHLYP/TZVP). The most Si–C bond stretching occurred between atoms Si(1) and C(2), to values ranging from 1.935 Å (BHLYP/TZVP) to 2.017 Å (B3LYP/TZVP). A simplified way to describe the structure **1a** relative to the ground state equilibrium geometry of **1** is to say that the environments of both silicon atoms have distorted part way from a tetrahedral to a trigonal bipyramidal geometry, in which the axial positions would be occupied by the $Me_3Si$ and in-plane methyl groups, and two of the equatorial positions by out-of-plane methyl groups. We shall see below that the third (in-plane) equatorial position is occupied by a non-bonding orbital of the "lone pair" type, but carrying only a small electron density.

As noted above, excited state vibrational analysis of **1a** revealed that only the structure obtained with the PBE0/TZVP method corresponds to an energy minimum on the $S_1$ surface. However, a relaxed C–Si–C angle surface scan showed even the PBE0/TZVP minimum to be extremely shallow, on the order of 10 $cm^{-1}$. The other methods (B3LYP/TZVP, BHLYP/TZVP, RIADC(2)/TZVP and RICC2/TZVP) found the lowest frequency to be imaginary, showing the stationary point as a transition state on the $S_1$ surface. Although the BHLYP and ab initio excited state vibrational calculations for the "blue" species **1a** indicate strongly that this $S_1$ stationary point is a transition state, the excitation energies and oscillator strengths obtained by these methods at this geometry fit expectations extrapolated from the permethylated oligosilane series, where both oscillator strengths and vertical emission energies decrease as the chain is shortened[7].

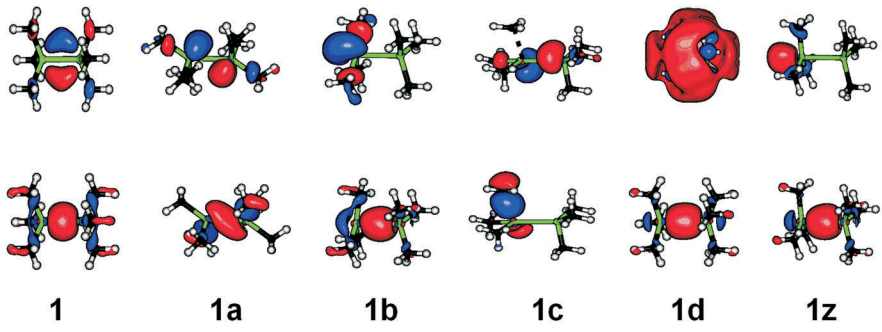


FIG. 2
B3LYP/def2-TZVP HOMO (bottom) and LUMO (top) for relaxed $S_1$ structures **1a–1c** and **1z**, plotted on the 0.06 isodensity contour value (for the LUMO of **1d**, 0.014). For **1**, the $\pi^*$ MO is shown instead of the LUMO, which is Rydberg

The $S_1$ excited state ($1A_u$) of the blue structure **1a** corresponds to a HOMO ($a_g$) to LUMO ($a_u$) $\sigma\sigma^*$ transition from the ground state. The excitation is delocalized equally over the two Si atoms. The LUMO is Si–Si antibonding, but also contains significant contributions from the hybrid orbitals of the in-plane C atoms that form the Si(1)–C(1) and Si(2)–C(6) bonds (Fig. 2), and a small contribution from an additional non-bonding mixed $4s,4p_z$ orbital on each Si atom, pointing into the large Si–Si–C angle. This fifth NHO on each silicon atom has an occupancy of only 0.06 $e^-$ in the $S_1$ state, which can be compared with an occupancy of 0.85 $e^-$ for the hybrid pointing to the other silicon atom. This fifth non-bonding orbital population represents only 2% of the total electron count in the Si valence orbitals. The hybrid orbitals used to make the Si–Si bond have increased p character ($sp^4$ in the PBE0/TZVP structure) and those used to make the Si(1)–C(1) and Si(2)–C(6) bonds have increased s character ($sp^2$ in the PBE0/TZVP structure). The $S_0$-$S_1$ electronic transition dipole moment lies along the Si–Si bond and the dipole moment of the $S_1$ state is zero.

The vertical emission energy of **1a** calculated with the B3LYP/def2-TZVP method is 25 470 $cm^{-1}$ at the minimum geometry obtained with TDDFT using the PBE0 functional and TZVP basis set. This corresponds to a large site distortion energy of 9 590 $cm^{-1}$ and a huge Stokes shift of 27 310 $cm^{-1}$.

*The Green Structure **1b***

This $C_s$ structure was obtained as a true minimum from the optimization and vibrational analysis of **1** with TDDFT using PBE0/TZVP, B3LYP and BHLYP functionals, and also with RIADC(2) and RICC2 methods (Table II). It resembles those proposed[52] to contribute to the green emission[15] of longer oligosilanes. However, like **1a**, this minimum is also quite shallow and a crude relaxed C–Si–Si angle scan yielded a barrier of only ~350 $cm^{-1}$ for **1b** going to the funnel **1β**.

The structure of **1b** contains a mirror plane that cuts through atoms C(2), Si(1), Si(2) and C(5), and two hydrogen atoms. The Si–Si bond length varies from 2.657 Å (PBE0/TZVP) to 2.734 Å (B3LYP/TZVP). The longest Si–C bonds are from Si(1) to C(1) and C(3). The Si(1)–C(1) bonds range from 1.958 Å (RIADC(2)/TZVP) to 2.008 Å (B3LYP/TZVP). Large geometrical rearrangements of C(1) and C(3) give rise to a very wide C–Si–C valence angle, ranging from 164.7° (B3LYP/TZVP) to 168.0° (RIADC(2)/TZVP) and to narrow C–Si–Si valence angles, ranging from 86.4° (RIADC(2)/TZVP) to 92.7° (B3LYP/TZVP). A simplified description is again possible by stating that in **1b** only one silicon atom deviates from tetrahedral toward trigonal

TABLE II
Structural parameters for the green minimum **1b**, optimized with various methods

| Structure | ∠C–Si–C, ° | ∠C–Si–Si, ° | Si–Si, Å | Si–C, Å |
|---|---|---|---|---|
| $Si_2Me_6$ | 112.7 | 107.5 | 2.657 | 1.881 |
| PBE0/TZVP | 112.7 | 103.9 | | 1.880 |
| $C_s$ | 111.9 | 107.5 | | 1.881 |
| **1b** | 165.3 | 92.4 | | 1.990 |
| | 96.2 | 92.4 | | 1.990 |
| | 96.2 | 103.2 | | 1.990 |
| $Si_2Me_6$ | 112.3 | 108.1 | 2.734 | 1.891 |
| B3LYP/TZVP | 112.3 | 103.9 | | 1.891 |
| $C_s$ | 111.6 | 108.1 | | 1.891 |
| **1b** | 164.7 | 92.7 | | 2.008 |
| | 96.5 | 92.7 | | 2.008 |
| | 96.5 | 101.6 | | 1.919 |
| $Si_2Me_6$ | 112.5 | 107.4 | 2.690 | 1.877 |
| BHLYP/TZVP | 112.5 | 105.0 | | 1.874 |
| $C_s$ | 111.5 | 107.4 | | 1.877 |
| **1b** | 167.2 | 90.1 | | 1.977 |
| | 95.9 | 90.1 | | 1.977 |
| | 95.9 | 112.6 | | 1.908 |
| $Si_2Me_6$ | 112.2 | 107.7 | 2.704 | 1.886 |
| RIADC(2)/TZVP | 112.2 | 106.0 | | 1.883 |
| $C_s$ | 110.7 | 107.7 | | 1.886 |
| **1b** | 168.0 | 86.4 | | 1.958 |
| | 95.8 | 86.4 | | 1.958 |
| | 95.8 | 112.9 | | 1.906 |
| $Si_2Me_6$ | 112.4 | 107.3 | 2.667 | 1.885 |
| RICC2/TZVP | 112.4 | 106.1 | | 1.882 |
| $C_s$ | 111.0 | 107.3 | | 1.885 |
| **1b** | 168.2 | 87.6 | | 1.967 |
| | 95.9 | 87.6 | | 1.967 |
| | 95.9 | 110.0 | | 1.910 |

bipyramidal symmetry, but much more than in **1a**, and almost reaches it (the C(1)–Si(1)–C(3) angle is 163°). This time, the axial positions are occupied by methyl groups, one of the equatorial positions by a $Me_3Si$ group, the second one by a methyl group, and the third one by a "non-bonding" orbital. As we shall see in a moment, this fifth silicon orbital carries about twice the electron density than it did in **1a**, where, however, there were two such orbitals, one on each silicon.

B3LYP/def2-TZVP calculations of the vertical emission energy of the green minimum **1b** are sensitive to the exact geometry and give different results depending on the $S_1$ optimization method. $S_1$ structures optimized with TDDFT give vertical emission energies from 16 620 $cm^{-1}$ (BHLYP/TZVP structure) to 17 700 $cm^{-1}$ (PBE0/TZVP structure). Those optimized with ab initio methods give lower values, from 13 780 $cm^{-1}$ for the RIADC(2)/TZVP structure to 14 880 $cm^{-1}$ for the RICC2/TZVP structure.

However, the nature of the excited state is similar for all the methods and involves an excitation from the Si–Si HOMO (*a*′) to the LUMO (*a*′), localized at the C(1)–Si(1) and Si(1)–C(3) bonds. The Si(1) hybrids pointed towards C(1) and C(3) are approximately $sp^2$ hybridized and have higher than average occupation. The hybrid pointed towards Si(2) has high p character (e.g., 99.8% $3p_x$ in the BHLYP/TZVP structure) and lower than average occupancy (0.52 $e^-$). While **1b** structures obtained with different methods were similar in terms of geometrical parameters, NHO hybridization values varied depending on the structures analyzed. NHO analysis of this excitation shows a removal of electron density from the orbitals forming the Si–Si bond, especially the hybrid on Si(1), and its movement to both a non-bonding fifth "valence" orbital located on Si(1) and to the Si(1)–C(1) and Si(1)–C(3) antibonding orbitals, in relative amounts that depend on the method used in the excited state optimization. TDDFT structures favored excitation into the Si–C antibonding orbitals, whereas ab initio methods favored excitation into a fifth valence orbital.

Surprisingly, according to our NHO analysis, the fifth valence atomic orbital on Si is made up of larger contributions from the 4s and 4p Si atomic orbitals and with smaller contributions from the Si 3d orbitals. This fifth valence orbital carried populations ranging from 0.09 to 0.18 $e^-$, which represent between 3 and 6% of the total electron count in the Si valence orbitals in the BHLYP and RICC2/TZVP structures, respectively. Also the other four valence hybrids contain notable contributions from the 4s and 4p orbitals, showing that the transfer of negative charge to the Si atom not only induces the addition of an orbital containing primarily contributions

with the next higher principal quantum number, but also causes a size expansion of the usual four hybrids already present.

The arrangement of the five valence orbitals on the Si(1) atom is approximately trigonal bipyramidal. The overall natural charge on the $Si(1)Me_3$ group is –0.32 (BHLYP/TZVP structure), and on the Si(1) atom, +1.14. The bonds carrying the four substituents are ordinary 2-electron bonds, each involving a single hybrid orbital on Si, and a NBO search did not locate a 3-center 4-electron bond. This makes the situation clearly distinct from those in the ground states of pentacoordinate silicon compounds, where each lobe of an Si 3p orbital is used to attach one axial substituent through a 3-center 4-electron bond.

The TDDFT $S_1$ structures have larger $S_1$ dipole moments (~3 Debye) and smaller oscillator strengths, from 0.005 (PBE0/TZVP structure) to 0.008 (BHLYP/TZVP structure) than those obtained with the ab initio methods (dipole moment of ~2 Debye and oscillator strengths of 0.014 at the RICC2/TZVP structure and 0.017 at the RIADC(2)/TZVP structure). The weak $S_0$-$S_1$ transition is polarized along the Si–Si bond. The ab initio **1b** structures have slightly smaller site distortion energies, cf. 13 780 $cm^{-1}$ for the PBE0/TZVP structure versus 12 990 $cm^{-1}$ for the RIADC(2)/TZVP structure. The ab initio **1b** minima have correspondingly larger ground state distortion (destabilization) energies, cf. 21 310 $cm^{-1}$ for the PBE0/TZVP structure versus 26 070 $cm^{-1}$ for the RIADC(2)/TZVP structure.

*The Si–C Stretch Structure **1c***

This structure was obtained only with the B3LYP/TZVP method and its label is derived from its 2.358 Å long Si(1)–C(1) bond, 25% longer than the 1.907 Å in the ground state (Fig. 1 and Table III). Its 2.745 Å Si–Si bond is 16% longer than in the ground state. The second longest (1.943 Å) Si–C bond, Si(1)–C(2), makes a wide C(2)–Si(1)–Si(2) valence angle of 156.3°. The Si(1) atom lies very close to the C(2), C(3) and Si(2) plane and the structure is approximately trigonal bipyramidal on Si(1), with a C(1)–Si(1)–C(2) angle of 91.7°, a C(1)–Si(1)–C(3) angle of 93.8°, and a C(1)Si(1)Si(2) angle of 95.8°. The $Me_3Si$, C(2) and C(3) substituents on Si(1) are equatorial, C(1) and a vacant site are axial.

The $S_1$ state of the Si–C bond stretch minimum **1c** is quite polar, with a dipole moment of 2.79 Debye, and the $S_0$-$S_1$ transition has a weak oscillator strength of 0.003. The HOMO of **1c** is located primarily on the stretched Si(1)–C(1) bond, and the LUMO mainly on the Si–Si bond (Fig. 2). More specifically, analysis of natural hybrid orbital populations shows that the

charges are localized almost exclusively on the Si(1) atom. Its hybrid orbital that points to the methyl carbon C(1) along the strongly stretched bond has a 99% p character and a low population density (0.31 $e^-$), and its hybrid that points to Si(2) along the Si–Si bond is approximately $sp^2$ in nature and has a high population density (1.36 $e^-$). The approximately $sp^2$ hybridization of the Si(1) atom fits the calculated trigonal bipyramidal geometry. In the first approximation, the structure can be described as a dimethylsilylene that makes a 3-electron bond to a trimethylsilyl radical through its lone pair and a one-electron bond to a methyl radical through its empty p orbital. An approximate label that could be attached to the $S_1$ state at the **1c** geometry then is $\pi\sigma^*$ local excitation at Si(1), plus considerable contributions from its neighbors.

TABLE III
Geometrical parameters for **1c**, **1d** and **1z**

| Structure | ∠C–Si–C, ° | ∠C–Si–Si, ° | Si–Si, Å | Si–C, Å |
|---|---|---|---|---|
| $Si_2Me_6$ | 105.6 | 95.0 | 2.745 | 1.917 |
| B3LYP/TZVP | 106.2 | 136.7 | | 1.935 |
| $C_1$ | 107.6 | 102.9 | | 1.914 |
| **1c** | 100.3 | 156.3 | | 1.943 |
| | 91.7 | 101.6 | | 1.913 |
| | 93.8 | 95.8 | | 2.358 |
| $Si_2Me_6$ | 119.2 | 95.2 | 2.797 | 1.884 |
| B3LYP/TZVP | 119.2 | 95.2 | | 1.884 |
| $C_3$ | 119.2 | 95.2 | | 1.884 |
| **1z** | 112.3 | 106.5 | | 1.888 |
| | 112.3 | 106.5 | | 1.888 |
| | 112.3 | 106.5 | | 1.888 |
| $Si_2Me_6$ | 116.4 | 101.1 | 2.708 | 1.876 |
| B3LYP/aug-cc-pVDZ | 116.4 | 101.1 | | 1.876 |
| $D_3$ | 116.4 | 101.1 | | 1.876 |
| **1d** | 116.4 | 101.1 | | 1.876 |
| | 116.4 | 101.1 | | 1.876 |
| | 116.4 | 101.1 | | 1.876 |

The B3LYP/def2-TZVP vertical emission energy is 17 100 $cm^{-1}$ (Table IV). The site distortion energy, 8 890 $cm^{-1}$, is slightly smaller than for **1a**, but the Stokes shift, 35 560 $cm^{-1}$, is even larger, due to a greater ground state destabilization at the relaxed $S_1$ geometry.

*The Rydberg Structure **1d***

This structure, very similar to that of the radical cation (cf. Supplementary Information), was obtained with the B3LYP/aug-cc-pVDZ method. Slight methyl rotations and C–Si–Si–C dihedral angles of 169.1° caused a deviation from $D_{3d}$ symmetry, resulting in an overall $D_3$ symmetry and no dipole moment for **1d**. The Si–Si bond length (2.708 Å) is elongated compared to the ground state (2.375 Å for B3LYP/aug-cc-pVDZ). The Si–C bonds (1.876 Å) are only slightly shorter than those in the ground state (1.907 Å). The C–Si–Si valence angles (101.1°) are slightly contracted when compared to those of the ground state (108.6°). The excitation is from the Si–Si HOMO and the terminal orbital is of 4s nature (Fig. 2). The transition from the ground state is forbidden. The site distortion is 7 530 $cm^{-1}$ and the calculated Stokes shift is 16 390 $cm^{-1}$.

*The Structure **1z***

A B3LYP/TZVP optimization of **1** led to the structure **1z** which belongs to the $C_3$ symmetry group. At 2.797 Å, the Si–Si bond is stretched more in this structure than in any other found. The 119.2° C–Si–C valence angle at Si(1) is slightly larger than those at Si(2), which are 112.3°. The C–Si(1)-Si(2) valence angles are smaller (95.2°) than those at the neighboring silicon, C–Si(2)-Si(1), which are closer to those of the ground state. The lengths of the Si–C bonds are almost identical. The structure is approximately trigonal bipyramidal on Si(1), with three equatorial methyl groups. The axial positions are taken by the $Me_3Si$ group and by a non-bonding orbital with low occupancy.

The valence state of structure **1z** is of σσ* nature and has a large $S_1$ dipole moment, 3.3 Debye. Its Si–C NHOs are approximately $sp^2$ hybridized and the NHO directed along the Si–Si axis a high $3p_x$ character. This reorganization is more pronounced on Si(1), which also carries some electron density (0.12 $e^-$) in an additional 4sp orbital in one of its axial positions. This hypervalent non-bonding orbital population represents 5% of the total electron count in the Si valence orbitals. The $S_1$ state of **1z** has the largest excitation energy of all the minima and stationary points considered,

29 960 $cm^{-1}$ when calculated with the B3LYP/def2-TZVP method. The transition from the ground to the valence state has a relatively sizeable oscillator strength of 0.049 and its transition dipole moment lies along the Si–Si bond. This state has a large site distortion energy of 11 100 $cm^{-1}$ but a relatively small Stokes shift of 22 700 $cm^{-1}$. When diffuse functions are added to the basis set, it no longer represents $S_1$, which is then represented by another state of Rydberg nature, whose further optimization causes the structure to collapse to the Rydberg structure **1d**. Reoptimization of **1z** with other methods can alternatively cause the structure to collapse into the green minimum **1b** (cf. Supplementary Information).

*Structures of Near $S_0$-$S_1$ Degeneracy, Funnels*

Geometry distortion along the lowest imaginary mode of the transition state **1a** on the $S_1$ surface led to a funnel connecting the $S_1$ and $S_0$ surfaces, exemplified by structure **1α** in Fig. 1. This structure is marked by an inverted C(1)–Si(1)–Si(2) bend of 213.8° (or new internal angle of 146.2°). There is also a large C–Si–C valence angle of 155.4° at C(2)–Si(1)–C(3). The corresponding C(2)–Si(1) and C(3)–Si(1) bonds are the longest at 1.965 and 1.982 Å, respectively. There is a small C(3)–Si(1)–Si(2) valence angle of 80.0°. The C(2)–Si(1)–C(1) and C(3)–Si(1)–C(1) angles are 92.9 and 91.5°, respectively.

The green minimum **1b** is stable with respect to reoptimization with all methods employed. If the structure is perturbed, however, a nearby $S_0$-$S_1$ funnel **1β** is found. Its structure is very similar to that of **1α** and differs only in an approximate 40° rotation of the Me groups on Si(2), the silicon atom that does not undergo rehybridization, in a direction that causes **1β** to have $C_s$ symmetry.

RIADC(2)/TZVP $S_1$ optimization of **1c** led to the funnel **1γ**. The optimization path seems to follow the stretching of the C(1) methyl group. The C(1)–Si(1) bond length of 2.358 Å in **1c** is extended to 2.525 Å in **1γ**, and the Si–Si bond length of 2.745 Å is shortened to 2.477 Å. In **1γ**, both C(2)–Si(1) and C(3)–Si(1) bonds are equally stretched to 1.922 Å. The C(1)–Si(1)–Si(2) bond angle is reduced from 95.8° in **1c** to 76.9° in **1γ**. The 157.0° C(2)–Si(1)–Si(2) angles in **1c** and **1γ** are similar (Fig. 3).

RIADC(2)/TZVP and RICC2/TZVP $S_1$ optimization of **1z** led to the funnel **1δ** with an extremely long Si–Si bond length of 3.471 Å. Opposing $SiMe_3$ groups are not completely symmetrical, the Si(1)–C bond lengths are slightly shortened (1.805 to 1.811 Å), and the Si(2)C bond lengths are slightly extended (1.941 to 1.944 Å). The C–Si(1)–Si(2) angles are also con-

tracted (76.9 to 77.0°) and the C–Si(1)–C angles are slightly increased (114.8 to 115.7°).

*Ground State Geometry Relaxation*

Since we have not identified the actual geometries of conical intersections, the structures of the funnels we found may well be biased toward one side and return through them will then favor products located on that side. Therefore, we do not attribute much significance to the product distribution that results from $S_0$ geometry optimization after return from a funnel and mention the results only briefly. CASSCF/6-31G* ground state optimization starting at the geometries **1α**, **1γ** and **1δ** returned the disilane to the ground state equilibrium geometry, **1**. A set of larger kicks to the funnel **1α**

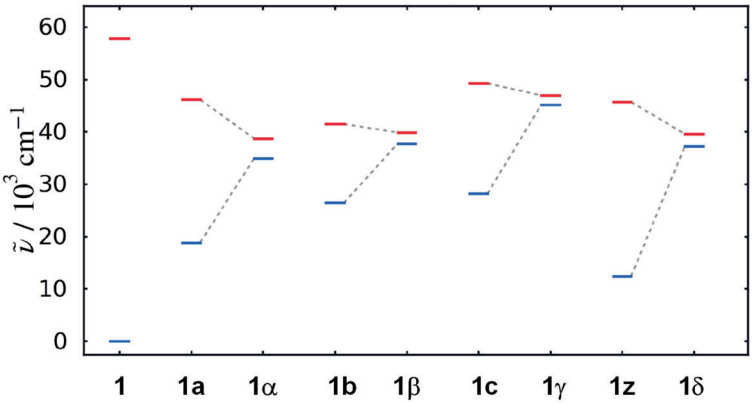


FIG. 3
RIADC(2)/TZVP plot of ground state equilibrium structure, and $S_1$ valence minima and funnels. Dashed lines do not necessarily imply the absence of barriers

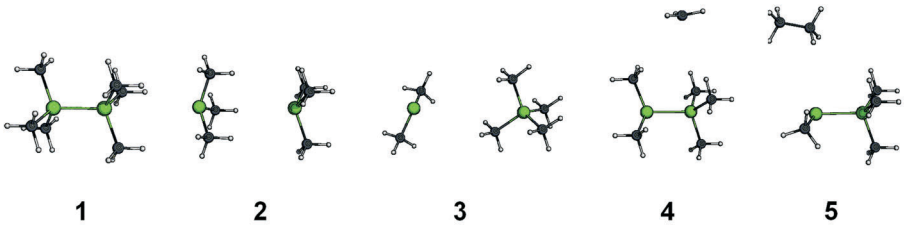


FIG. 4
Ground state return products (**1**–**5**) from funnels resulting from the CASSCF stochastic search method

gave mostly **1**, but also new products: the homolytic Si–Si cleavage product **2** and the dimethylsilylene extrusion plus tetramethylsilane product **3** (Fig. 4). When even larger kicks were given to the Si and C atoms, a small portion of the optimizations returned to **2**, **3**, and new dissociation products, a methyl plus $Me_2Si_2Me_3$ radical pair **4**. Larger kicks to the funnel **1γ** mostly returned to **1** but in rare cases produced **3**, **4** and a new product **5**, ethane plus the silylene $MeSiSiMe_3$. Return through the funnel **1δ** produced **1** and in one case, the product **2**.

*Comparison of Computational Methods*

The B3LYP/def2-TZVP vertical emission energies $E_{VE}$, site distortion energies $E_{SD}$, and Stokes shifts $E_{SS}$ at each relaxed $S_1$ structure are listed in Table IV.

TABLE IV
Vertical emission energies and oscillator strengths (B3LYP/def2-TZVP) for stationary points on the $S_1$ surface of hexamethyldisilane. $E_{SD}$ (site distortion energy) and $E_{SS}$ (Stokes shift) are calculated with reference to $S_0$ structures optimized with the method that was used for $S_1$ optimization

| Structure | Method[a] | State | $E_{VE}$ $cm^{-1}$ | $f$ | $E_{SD}$ $cm^{-1}$ | $E_{SS}$ $cm^{-1}$ | $S_1$ Dipole Debye |
|---|---|---|---|---|---|---|---|
| **1a** | PBE0 | $1A_u$ σσ* | 25 470 | 0.044 | 9 590 | 27 310 | 0.00 |
| | B3LYP | $1A_u$ σσ* | 25 430 | 0.041 | 9 370 | 27 230 | 0.00 |
| | BHLYP | $1A_u$ σσ* | 27 500 | 0.077 | 9 740 | 25 380 | 0.00 |
| | RIADC(2) | $1A_u$ σσ* | 24 360 | 0.073 | 9 760 | 28 480 | 0.00 |
| | RICC2 | $1A_u$ σσ* | 24 600 | 0.068 | 9 780 | 28 250 | 0.00 |
| **1b** | PBE0 | 2A′ σσ* | 17 700 | 0.005 | 13 780 | 35 090 | 3.58 |
| | B3LYP | 2A′ σσ* | 17 140 | 0.005 | 13 680 | 35 520 | 3.60 |
| | BHLYP | 2A′ σσ* | 16 620 | 0.008 | 13 860 | 36 260 | 3.23 |
| | RIADC(2) | 2A′ σσ* | 13 780 | 0.017 | 12 990 | 39 060 | 1.88 |
| | RICC2 | 2A′ σσ* | 14 880 | 0.014 | 13 320 | 37 970 | 2.32 |
| **1c** | B3LYP | 2A πσ* | 17 100 | 0.003 | 8 890 | 35 560 | 2.79 |
| **1d** | B3LYP[b] | $2A_1$ σ4s | 28 470 | 0.000 | 7 530 | 16 390 | 0.02 |
| **1z** | B3LYP | 2A σσ* | 29 960 | 0.049 | 11 100 | 22 700 | 3.26 |

[a] The TZVP basis set was used to obtain $S_1$ stationary points in conjunction with methods listed. [b] This state is of high Rydberg character and calculations used the aug-cc-pVDZ basis set.

Because the TDDFT method with standard functionals is known to underestimate the energies of Rydberg and charge transfer (CT) excited states, the excited state energies for the $S_1$ minima were checked with various methods. The resulting vertical emission energies are summarized in Table V.

TDDFT energies and oscillator strengths are compared to the results of the ab initio method, RICC2, which is better suited for the description of Rydberg or CT states. The RICC2/def2-TZVP method tends to overestimate excited state excitation energies of **1** (by approximately 2 400 $cm^{-1}$) when compared to experimental values (cf. Supplementary Information).

The advantage of the def2-TZVP-mD basis set is apparent in the results for the diffuse $S_1$ states of **1d** and **1z**. For these structures the presence of diffuse functions in the basis set alters the $S_1$ vertical emission energy significantly. For **1d** and **1z** the RICC2 emission energy dropped by 6 120 and 3 840 $cm^{-1}$, respectively, when using the def2-TZVP-mD basis instead of def2-TZVP (Table V). As noted above, the nature of the $S_1$ state of **1z** depends on the basis set used. With the def2-TZVP-mD basis set, the first excited state is of strongly Rydberg character, and with the def2-TZVP basis set, which lacks the diffuse functions, it is a valence excited state (Fig. 2). The addition of diffuse basis functions does not change the nature of the $S_1$ state of structures **1a**, **1b** and **1c**, and does not have a significant effect on their vertical emission energies $E_{VE}$. The $S_1$ of **1d** has a strong Rydberg character regardless of the basis set used. It needs to be noted, however, that while the addition of diffuse functions changes the $E_{VE}$ value at the struc-

TABLE V
Vertical emission energy $E_{VE}$ ($cm^{-1}$)

| Method | **1a** PBE0 | **1b** PBE0 | **1b** BHLYP | **1b** RIADC(2) | **1c** B3LYP | **1d** B3LYP | **1z** B3LYP |
|---|---|---|---|---|---|---|---|
| B3LYP/Def2-TZVP-mD | 25 330 | 17 340 | 16 270 | 13 440 | 17 020 | 28 310 | 26 290 |
| CAMB3LYP/Def2-TZVP-mD | 27 140 | 19 740 | 18 380 | 14 800 | 20 490 | 32 970 | 30 540 |
| LC-BLYP/Def2-TZVP-mD | 27 210 | 20 400 | 18 970 | 15 190 | 21 860 | 34 670 | 32 020 |
| LC′-BLYP/Def2-TZVP[a] | 25 300 | 18 260 | 17 080 | 13 920 | 18 700 | 34 590 | 31 180 |
| LC′-BLYP/Def2-TZVP-mD[a] | 25 220 | 17 980 | 17 000 | 13 650 | 18 690 | 30 241 | 28 090 |
| RICC2/Def2-TZVP | 28 350 | 21 230 | 18 970 | 15 550 | 21 430 | 38 400 | 33 390 |
| RICC2/Def2-TZVP-mD | 28 190 | 20 770 | 19 320 | 15 160 | 21 350 | 32 280 | 29 550 |
| RICC2/aug-cc-pVTZ | 28 130 | 20 940 | 19 760 | 15 400 | 21 400 | 32 330 | 29 640 |

[a] The μ parameter is set to 0.23 $a_0^{-1}$ for this LC-BLYP calculation, as opposed to the default value of 0.33 $a_0^{-1}$.

ture **1b** at most by 370 $cm^{-1}$, the diffuse functions have a significant effect when the geometry of **1b** is reoptimized, and this in turn can affect the $E_{VE}$ value by as much as ~2 000 $cm^{-1}$. For example, the LC'-BLYP/def2-TZVP $E_{VE}$ is **1** 700 $cm^{-1}$ higher at the B3LYP/aug-cc-pVTZ optimized than the B3LYP/TZVP optimized **1b** structure (all $E_{VE}$ values quoted correspond to a ground to valence σσ* state transition).

The TDDFT (B3LYP/def2-TZVP-mD and LC'-BLYP/def2-TZVP-mD) emission energies for the TDDFT PBE0/TZVP optimized blue structure **1a** are nearly identical, 25 330 and 25 220 $cm^{-1}$, respectively. The species **1c**, **1d** and **1z** did however show disparities between the standard TDDFT and the LC-TDDFT values, with differences of 1 600, 1 930 and 1 800 $cm^{-1}$, respectively (def2-TZVP-mD). There are also trends in the $S_0$-$S_1$ oscillator strengths of the different structures when calculated with various methods, with the RICC2 method consistently yielding the largest oscillator strengths for all structures (Table VI).

TABLE VI
Calculated $S_0$-$S_1$ oscillator strength

| Method | **1a** PBE0 | **1b** PBE0 | **1b** BHLYP | **1b** RIADC(2) | **1c** B3LYP | **1d** B3LYP | **1z** B3LYP |
|---|---|---|---|---|---|---|---|
| B3LYP/Def2-TZVP-mD | 0.045 | 0.004 | 0.007 | 0.015 | 0.003 | 0.000 | 0.013 |
| CAMB3LYP/Def2-TZVP-mD | 0.055 | 0.004 | 0.007 | 0.015 | 0.007 | 0.000 | 0.022 |
| LC-BLYP/Def2-TZVP-mD | 0.056 | 0.004 | 0.007 | 0.014 | 0.010 | 0.000 | 0.030 |
| LC'-BLYP/Def2-TZVP[a] | 0.045 | 0.005 | 0.007 | 0.015 | 0.005 | 0.000 | 0.060 |
| LC'-BLYP/Def2-TZVP-mD[a] | 0.045 | 0.004 | 0.007 | 0.014 | 0.005 | 0.000 | 0.020 |
| RICC2/Def2-TZVP | 0.066 | 0.008 | 0.013 | 0.027 | 0.008 | 0.000 | 0.093 |
| RICC2/Def2-TZVP-mD | 0.068 | 0.007 | 0.011 | 0.025 | 0.008 | 0.000 | 0.024 |
| RICC2/aug-cc-pVTZ | 0.067 | 0.007 | 0.012 | 0.026 | 0.008 | 0.000 | 0.025 |

[a] The μ parameter is set to 0.23 $a_0^{-1}$ for this LC-BLYP calculation, as opposed to the default value of 0.33 $a_0^{-1}$.

*The Λ Parameter*

The lambda parameter, Λ [53], is related to the integral of the moduli of the overlap between orbitals involved in an excitation (in this work, $S_0$-$S_1$), and is an indicator of charge transfer and Rydberg excited states. The Λ value of **1d** and **1z** depends the most on the basis set used (Table VII).

The blue minimum **1a** has the largest average Λ value, 0.59, nearly independent of the basis set or method used. The structure **1c** has a lower aver-

age Λ value of 0.46, also independent of the basis set or method. The diffuse minima **1d** and **1z** show a strong basis set dependence. Without diffuse basis set functions their respective Λ values are 0.51 and 0.38, and when calculated with the LC-B3LYP/Def2-TZVP-mD method, they drop to 0.28 and 0.23, respectively.

An interesting trend appears with the green minimum **1b**. The average Λ values for the $S_1$-$S_0$ transition increased for the structures obtained with more Hartree–Fock exchange in the functional used. For the **1b** structure obtained with the least amount of Hartree–Fock exchange, PBE0, the average Λ value was 0.44, for intermediate exchange in the BHLYP structure the average Λ value was 0.47, and the RIADC(2) structure gave the largest average Λ value of 0.55. Augmentation of the basis set used for the vertical emission energy calculation did not significantly alter the emission energy. An increase in the vertical $S_0$-$S_1$ ($\sigma\sigma^*$) energy difference at the **1b** structure is however observed if additional basis set augmentation is used in the TDDFT (B3LYP) excited state geometry optimizations.

TABLE VII
Λ dependence on TDDFT and LC-TDDFT methods

| Method | **1a** PBE0 | **1b** PBE0 | **1b** BHLYP | **1b** RIADC(2) | **1c** B3LYP | **1d** B3LYP | **1z** B3LYP |
|---|---|---|---|---|---|---|---|
| B3LYP/def2-TZVP | 0.62 | 0.49 | 0.52 | 0.60 | 0.46 | 0.38 | 0.51 |
| B3LYP/def2-TZVP-mD | 0.61 | 0.48 | 0.51 | 0.59 | 0.46 | 0.29 | 0.37 |
| CAMB3LYP/def2-TZVP-mD | 0.59 | 0.44 | 0.47 | 0.55 | 0.47 | 0.24 | 0.29 |
| LC-BLYP/def2-TZVP-mD | 0.53 | 0.48 | 0.52 | 0.59 | 0.48 | 0.37 | 0.28 |
| LC′-BLYP/def2-TZVP[a] | 0.61 | 0.43 | 0.46 | 0.54 | 0.46 | 0.25 | 0.49 |
| LC′-BLYP/def2-TZVP-mD[a] | 0.58 | 0.43 | 0.46 | 0.54 | 0.46 | 0.25 | 0.30 |

[a] The μ parameter is set to 0.23 $a_0^{-1}$ for this LC-BLYP calculation, as opposed to the default value of 0.33 $a_0^{-1}$.

## DISCUSSION

Until relatively recently, an attempt to survey the $S_1$ minima and $S_0$-$S_1$ funnels in a molecule of the size of $Si_2Me_6$ would have been hopeless, especially given that there are many closely spaced valence and Rydberg states at the ground state equilibrium geometry **1** [27], and that large bond-stretching and valence angle rearrangements often require multireference methods[54]. Even with today's computers, we were only able to perform this survey in a reasonable time because it turned out that at the stationary points found in this work a single excitation dominates and multireference

methods do not need to be used. The results obtained with different single-reference methods, DFT and ab initio, agreed with each other surprisingly well, and all led us to stationary points of rather similar structures. The situation is less favorable in the case of conical intersections, where multi-reference methods are mandatory. We have therefore not attempted to pinpoint their geometrical structures exactly, and have satisfied ourselves with identifying the approximate general regions of geometries in which they occur. We refer to such regions of near $S_0$-$S_1$ degeneracy as funnels in $S_1$ since we believe that they will usually induce a return to $S_0$ before the molecule has time to find the actual conical intersection point. Therefore, their knowledge should be sufficient for understanding when rapid return from $S_1$ to $S_0$ will occur and fluorescence from $S_1$ will be quenched. It is not sufficient for the prediction of efficiencies with which the various minima in $S_0$ will ultimately be reached and thus of the nature and quantum yields of the products. Such an examination would require a study of the molecular dynamics on the $S_1$ and $S_0$ surfaces with $S_1$-$S_0$ jumps considered explicitly. This kind of treatment lies beyond the scope of the present study and is not needed to answer the question posed in the title.

*Stationary Points in the $S_1$ State*

The density functional and ab initio methods converged to several stationary structures in the $S_1$ state of hexamethyldisilane, quite independently of which method was used. One of the structures (**1a**) appears to be a transition state, or possibly an extremely shallow minimum, and three others (**1b–1d**) are minima. We have also found four funnels, **1α–1δ**, loosely associated with these minima. Finally, we have identified a structure (**1z**) that is not a stationary point when diffuse functions are present in the basis set but turns into a minimum when they are absent. It may therefore possibly be of interest for studies on hexamethyldisilane in condensed media, in which Rydberg states are pushed up in energy and are normally not observed at all.

An oversimplified but useful overall characterization of the electronic wave functions at the stationary points on the $S_1$ surface is to say that they are of two types, primarily charge-pair and primarily dot-dot (often called zwitterionic and covalent, respectively), similarly as states of π-electron systems (e.g., analogous to the lowest excited $B_u$ and $A_g$ states of 1,3-butadiene). The former are more often associated with minima in $S_1$ and both are associated with conical intersections. In charge-pair minima or stationary states, the molecular geometry is distorted in a way that accommodates

the negative and the positive charge most readily and at the closest possible distance from each other. One way to proceed is to place the hole into the HOMO and the electron into a Rydberg orbital, as in **1d**. When we ask how to find optimal valence structures, a localization of both charges on the same atom is the best that can be done. Since the silicon atom has both a lower ionization potential and a higher electron affinity than a carbon atom, it is hardly surprising that both charges tend to localize on Si. Placing an empty orbital and a lone pair orbital on Si produces a silylene-like structure, and indeed in the first approximation the optimized minima tend to have an $sp^2$ hybridization and trigonal bipyramidal hybridization on one of the Si atoms.

In the "blue minimum" **1a**, whose structure resembles the bond stretch minima of longer oligosilane chains[52], both the bonding and the antibonding MO reside on both Si–Si and Si–C orbitals, and excitation is localized equally on both silicon centers. In hexamethyldisilane, this structure is a transition state or an extremely shallow minimum, depending on the method of calculation. A simple bending of the methyl groups conveys the excited molecule to the funnel **1α**, which then takes it to the ground state $S_0$. One final outcome is the relaxed $S_0$ equilibrium geometry **1**, and the ground-state products **2**, **3** and **4** may perhaps also result.

In any event, in hexamethyldisilane **1a** does not represent a region of geometries where the excited molecule is likely to sojourn for long. Its significance lies primarily in providing a conceptual bridge to the longer oligosilanes, in which this type of structure gradually becomes a significant minimum relative to nearby funnels as the chain becomes longer, and which is believed[52] to be responsible for the blue emission. It is a reasonable guess that the gradual accentuation of the blue minimum upon chain extension is due to an increased energy of the HOMO, from which electron density in this excitation is taken, whereas the energy of the dot-dot states that dominate in the vicinity of nearby funnels is affected less. A more detailed investigation of this point requires calculations for the longer oligosilanes[52].

The vertical emission energies of the structures of **1a** obtained with the various methods, e.g., 25 470 $cm^{-1}$ with the PBE0/TZVP method, are in line with experimental fluorescence energy extrapolation (24 700 $cm^{-1}$) from longer oligosilanes[7]. This close agreement is likely due to the high Λ value for the transition, indicating accurate reproduction of the **1a** structure and emission energy with traditional TDDFT methods.

The "green" structure **1b** is striking by its 3spd/4sp hybridization on Si(1) that results in the presence of five valence orbitals, four used to carry sub-

stituents and the fifth to carry a weakly occupied non-bonding "lone pair" that accommodates some of the negative charge transferred to this Si atom from the HOMO, the rest being accommodated in the Si(1)–C and Si–Si antibonding orbitals. The presence of such a somewhat diffuse but still clearly valence non-bonding fifth hybrid orbital on Si(1) with significant electron density implies hypervalency. While this non-bonding orbital has a low occupancy and carries only about 5% of the total valence electron count, its presence has large effects on the molecular geometry. Similar expansion of the Si valence shell to five or even six hybrid orbitals using orbitals of the 3d shell used to be invoked commonly for the ground states of various compounds containing a pentacoordinate or hexacoordinate Si atom, but more recent calculations showed convincingly that in these structures a Si atom uses only four hybrid orbitals and carries no more than eight electrons in its valence shell[55–57]. Qualitatively, it is much more acceptable to postulate such a participation by high-energy orbitals in an expansion of the valence shell of a high-energy excited state, but this result is still quite remarkable.

Examination of the $S_1$ emission energies, $S_0$-$S_1$ oscillator strengths, and $S_0$-$S_1$ $\Lambda$ values (Tables III–VII) of the structures of **1b** obtained by ab initio and TDDFT methods provides interesting insight. Since $S_1$ of **1b** has some amount of charge transfer character, the large difference between B3LYP and LC'-BLYP emission energies is likely caused by artificial charge transfer contamination. As seen in **1c**, diffuse functions do not significantly change the emission energy. Additional HF exchange helps to correct the artificial charge transfer problem in TDDFT. Emission energies from the ab initio RIADC(2) **1b** structure are lower than that of the PBE0 TDDFT **1b** structure. Emission energies from various methods for the **1b** structure obtained with BHLYP functional are between those of the PBE0 and RIADC(2) **1b** structures, in accord with the intermediate HF exchange of the BHLYP functional. A similar trend is followed with the $S_0$-$S_1$ oscillator strengths and the $\Lambda$ values. The $\Lambda$ values for the **1b** PBE0 structure are not very low, but result in largely different emission energies than those of the ab initio structures. Because the emission calculations were done with various methods, including ab initio methods, it means that the effects of artificial charge transfer have apparently been built into the optimized structures. The **1b** PBE0 structures had an average emission of 19 100 $cm^{-1}$ whereas the average emission energy for the **1b** RIADC(2) structure is much less at 14 550 $cm^{-1}$. For the **1b** RIADC(2) structure the traditional TDDFT excitation energy does not vary significantly from the LC'-BLYP result, most likely because effects of artificial charge transfer have not been built into this structure.

The $S_1$ excited state at the Si–C bond stretch structure **1c** has some charge transfer character and a reduced Λ parameter when compared to **1a**. The B3LYP/def2-TZVP-mD and LC-BLYP/def2-TZVP-mD emission energies now differ by 1 670 $cm^{-1}$. As diffuse functions do not significantly change the calculated emission energy, this difference is attributed to the partial charge transfer character of the transition. It is suspicious that this minimum only appears in TDDFT calculations with functionals with little or no HF exchange, and one must wonder whether it is an artifact due to a poor treatment of charge transfer in such methods.

As expected, basis set choice had a large impact on the emission energy of the Rydberg minimum **1d**, and even in the absence of diffuse functions the $S_1$ state was Rydberg. This is partially evident in the persistently low Λ value for **1d**. The LC-BLYP value differs slightly more (2 040 $cm^{-1}$) from the RICC2 value for **1d** than is the case for **1z** (1 460 $cm^{-1}$). This can be due to the μ parameter which was optimized to reproduce a valence excited state and not a Rydberg excited state.

Excitation in **1z**, too, is localized at Si(1) in a silylene-like fashion when diffuse functions are not used in the calculation. As diffuse functions are added to the basis set, it gradually acquires Rydberg character. Further optimization with diffuse basis sets leads to the Rydberg minimum **1d**. It is possible that this will not happen to **1z** in solution, and then **1z** could be regarded as an intermediate to the more localized green minimum **1b**.

*Funnels*

According to the single reference methods utilized in this work, the disilane can reorganize to find the funnels, **1α**, **1β**, **1γ** and **1δ**. The asymmetric distortion of the hexamethyldisilane clearly disrupts the equal weights of the zwitterionic charge pair valence bond description of the **1a** σσ* mixed state, giving rise to a heterosymmetric biradicaloid, which is expected[1] to result in a conical intersection, **1α** and **1β**. These structures resemble those of the alkene analog, the twisted monopyramidalized conical intersection for ethylene which has been found with multireference methods[58].

Ground state optimization starting at the various funnel structures mostly returned the molecule to **1**, the ground state minimum energy $D_{3d}$ structure. As noted, there could be a systematic bias in this result and a more thorough investigation might reveal that the photoproducts that were located, homolytic Si–Si bond cleavage product **2**, a silylene extrusion plus tetramethylsilane product **3**, methyl dissociation product **4** and the ethane plus silylene product **5**, are formed more often. Overall, these prod-

ucts seem quite reasonable. The silylene in product **5** is known to rapidly convert to silene[25]. Products **2**, **3** and **5** are expected from processes known in longer oligosilane chains[6]. Product **4** is not commonly believed to be involved in the photochemical decomposition of oligosilanes[25].

Why do disilanes and trisilanes not emit, while longer oligosilanes do? Although we have only made crude scans, it is clear that in hexamethyldisilane, the barriers around the blue and green minima are very small. Relaxed C–Si–C angle scans yielded barriers of 10 and ~350 $cm^{-1}$ for **1a** and **1b** going to **1α** and **1β**, respectively. Site distortion energies are huge and after vertical excitation a large amount of electronic potential energy will be converted into kinetic energy of the nuclei and will allow the molecule to explore large regions of its potential energy surface. While minima might be accessed it may only be momentarily and given the weak oscillator strengths at the minima, it is no wonder that fluorescence has a difficult time competing.

As one proceeds to longer chains, the situation will improve. Both the blue minimum **1a** and the green minimum **1b** involve excitation of an electron from the HOMO and are likely to benefit energetically relative to nearby funnels in longer oligosilanes. We propose that a gradual disappearance of significant minima of this type as the peralkylated silicon chain is shortened is responsible for the concommitant gradual decrease of the quantum yield of both the blue and the green fluorescence. Emission is already quite weak in the tetrasilane, and is undetectable in both trisilane and disilane.

## SUMMARY

Valence state minima in the $S_1$ surface of hexamethyldisilane located by TDDFT and ab initio methods are extremely shallow and are accompanied by nearby funnels that return the molecule to the $S_0$ surface, accounting for the absence of fluorescence. These minima, particularly the "blue" minimum **1a** and the "green" minimum **1b**, are significant in that they provide models for excitation localization in somewhat longer peralkylated oligosilane chains, which emit in the blue and green. They are also important in that they provide insight into the nature of the very substantial geometrical distortions experienced by saturated molecules in the excited singlet states. In a nutshell, minima occur at geometries capable of accommodating a negative and a positive charge close to each other. Placement of both on the same silicon atom produces an approximately trigonal bipyramidal geometry that allows the Si atom to still carry four substituents yet also have a

fifth site for a positive or a negative charge. In **1c**, the electronic structure on one of the silicon atoms is silylene-like and contains an empty p orbital and a doubly occupied hybrid orbital of roughly $sp^2$ character. In **1a**, **1b** and **1z**, four of the vertices of a trigonal bipyramid are occupied by substituents and the fifth by a weakly occupied non-bonding "lone–pair" type orbital. Although it carries only a few per cent of the valence electron count, this orbital has a significant effect on the molecular geometry. The presence of five valence orbitals on a silicon atom, especially clear in **1b**, makes this atom hypervalent and permits it to accommodate the negative charge taken from the HOMO, partly as a "lone pair" and partly in the antibonding orbitals of the Si–C and Si–Si bonds.

A considerably oversimplified comparison of the most important structures discovered, the blue structure **1a** and the green structure **1b**, in their $S_1$ states may be instructive. Compared with the ground state equilibrium geometry **1**, in which both Si atoms are tetrahedral and $sp^3$ hybridized, **1a** keeps the excitation delocalized symmetrically on both Si atoms by distorting both half-way toward a trigonal bipyramidal geometry, whereas **1b** distorts only one of them, but almost all the way to a trigonal bipyramid. In **1a**, the axial positions are occupied with $Me_3Si$ and a methyl, and the equatorial positions with two methyls and a hypervalent fifth valence orbital of primarily 4sp character with some 3d admixture. The fifth orbital carries some of the excess negative charge that was removed from the HOMO and the rest goes into the Si–Si and Si–C antibonding orbitals. In **1b**, the axial positions are occupied with methyls and the equatorial positions with a methyl, a $Me_3Si$, and a fifth valence orbital carrying as much electron population as the two such orbitals do in **1a**.

The original proposal that the blue emitting minimum is characterized by an Si–Si bond stretch thus needs to be elaborated by specifying that in hexamethyldisilane an Si–C bond is stretched even more and that valence angles are distorted in the direction of making the silicon atoms trigonal bipyramidal. It remains to be seen what the exact geometries of the blue minima are in somewhat longer oligosilanes.

The $S_1$ structures obtained with TDDFT methods depend considerably on the choice of functional and only sometimes gave similar results as the ab intio methods (RICC2 and RIADC(2)), e.g., for **1b**. Analysis of $\Lambda$ parameter values and differences in excitation energies for the various excited state minima shows that TDDFT excited state optimizations require extreme caution as effects of artificial charge transfer can be built into the structure. This seems like only a minor problem for hexamethyldisilane, but could increase in importance as the size of the oligosilane is increased.

*This work was supported by U.S. National Science Foundation grant CHE 0848477.*

**REFERENCES**

1. Michl J., Bonačić-Koutecký V.: *Electronic Aspects of Organic Photochemistry*. John Wiley & Sons, New York 1990.
2. Salem L., Dauben W. G., Turro N.: *Acc. Chem. Res.* **1975**, *8*, 41.
3. Michl J.: *Topics Curr. Chem.* **1974**, *46*, 1.
4. Hirayama F., Lipsky S.: *J. Chem. Phys.* **1969**, *51*, 3616.
5. Michl J., West R.: *Acc. Chem. Res.* **2000**, *33*, 821.
6. Miller R. D., Michl J.: *Chem. Rev.* **1989**, *89*, 1359.
7. Raymond M. K., Michl J.: *Int. J. Quantum Chem.* **1999**, *72*, 361.
8. Kim Y. R., Lee M., Thorne J. R. G., Hochstrasser R. M., Zeigler J. M.: *Chem. Phys. Lett.* **1988**, *145*, 75.
9. Schepers T., Michl J.: *J. Phys. Org. Chem.* **2002**, *15*, 490.
10. Bande A., Michl J.: *Chem. Eur. J.* **2009**, *15*, 8504.
11. Michl J.: *Acc. Chem. Res.* **1990**, *23*, 127.
12. Rooklin D., Schepers T., Raymond-Johansson M., Michl J.: *Photochem. Photophys. Sci.* **2003**, *2*, 511.
13. Raymond M. K., Magnera Th. F., Zharov I., West R., Dreczewski B., Nozik A. J., Sprague J. R., Ellingson R. J., Michl J. in: *Applied Fluorescence in Chemistry Biology and Medicine* (W. Rettig, B. Strehmel, C. Schrader and H. Seifert, Eds). Springer, Berlin 1999.
14. Fogarty H., Casher D., Imhof R., Schepers T., Rooklin D., Michl J.: *Pure Appl. Chem.* **2003**, *75*, 999.
15. Fogarty H.: *Ph. D. Thesis*. University of Colorado, Boulder 2005.
16. Plitt H., Balaji V., Michl J.: *Chem. Phys. Lett.* **1993**, *213*, 158.
17. Mazières S., Raymond M. K., Raabe G., Prodi A., Michl J.: *J. Am. Chem. Soc.* **1997**, *119*, 6682.
18. Olivucci M., Robb M. A., Bernardi F. in: *Conformational Analysis of Molecules in Excited States* (J. Waluk, Ed.). Wiley–VCH, New York 2000.
19. Karatsu T., Miller R. D., Sooriyakumaran R., Michl J.: *J. Am. Chem. Soc.* **1989**, *111*, 1140.
20. Ishikawa M., Takaoka T., Kumada M.: *J. Organomet. Chem.* **1972**, *42*, 333.
21. Drahak T., Michl J., West R.: *J. Am. Chem. Soc.* **1979**, *101*, 5427.
22. Moiseev A. G., Leigh W.: *J. Organometallics* **2007**, *26*, 2677.
23. Michl J., Balaji V. in: *Computational Advances in Organic Chemistry: Molecular Structure and Reactivity* (C. Ögretir and I. Csizmadia, Eds). Kluwer Academic Publishers, Dordrecht 1991.
24. Venturini A., Vreven T., Bernardi F., Olivucci M., Robb M. A.: *Organometallics* **1995**, *14*, 4953.
25. McKinley A. J., Karatsu T., Wallraff G. M., Thompson D. P., Miller R. D., Michl J.: *J. Am. Chem. Soc.* **1991**, *113*, 2003.
26. Casher D. L., Tsuji H., Sano A., Katkevics M., Toshimitsu A., Tamao K., Kubota M., Kobayashi T., Ottosson C. H., David D. E., Michl J.: *J. Phys. Chem. A* **2003**, *107*, 3559.
27. Piqueras M. C., Crespo R., Michl J.: *J. Phys. Chem. A* **2008**, *112*, 13095.
28. Teramae H., Michl J.: *Chem. Phys. Lett.* **1997**, *276*, 127.
29. Becke A. D.: *J. Chem. Phys.* **1993**, *98*, 5648.

30. Perdew J. P., Ernzerhof M., Burke K.: *J. Chem. Phys.* **1996**, *105*, 9982.
31. Adamo C., Barone V.: *J. Chem. Phys.* **1999**, *110*, 6158.
32. Becke A. D.: *J. Chem. Phys.* **1993**, *98*, 1372.
33. Schafer A., Huber C., Ahlrichs R.: *J. Chem. Phys.* **1994**, *100*, 5829.
34. Dunning T. H.: *J. Chem. Phys.* **1989**, *90*, 1007.
35. *TURBOMOLE*, V6.2 2010, A Development of University of Karlsruhe and Forschungszentrum Karlsruhe GmbH, 1987–2007. TURBOMOLE GmbH, since 2007, available from http://www.turbomole.com.
36. Hättig C., Weigend F.: *J. Chem. Phys.* **2000**, *113*, 5154.
37. Hättig C. in: *Response Theory and Molecular Properties (A Tribute to Jan Linderberg and Poul Jørgensen)* (J. R. Sabin, E. Brändas, H. Jensen, Eds.), *Advances in Quantum Chemistry*, Vol. 50, pp. 37–60. Academic Press, New York 2005
38. Weigend F., Häser M., Patzelt H., Ahlrichs R.: *Chem. Phys. Lett.* **1998**, *294*, 143.
39. Vosko S. H., Wilk L., Nusair M.: *Can. J. Phys.* **1980**, *58*, 1200.
40. Treutler O., Ahlrichs R.: *J. Chem. Phys.* **1994**, *102*, 346.
41. Furche F., Ahlrichs R.: *J. Chem. Phys.* **2002**, *117*, 7433.
42. Hättig C.: *J. Chem. Phys.* **2003**, *118*, 7751.
43. Köhn A., Hättig C.: *J. Chem. Phys.* **2003**, *119*, 5021.
44. Yanai T., Tew D., Handy N.: *Chem. Phys. Lett.* **2004**, *393*, 51.
45. Tawada Y., Tsuneda T., Yanagisawa S., Yanai T., Hirao K.: *J. Chem. Phys.* **2004**, *120*, 8425.
46. Schmidt M. W., Baldridge K. K., Boatz J. A., Elbert S. T., Gordon M. S., Jensen J. H., Koseki S., Matsunaga N., Nguyen K. A., Su S. J., Windus T. L., Dupuis M., Montgomery J. A.: *J. Comput. Chem.* **1993**, *14*, 1347.
47. Papajak E., Leverentz H. R., Zheng J., Truhlar D. G.: *J. Chem. Theory Comput.* **2009**, *5*, 1197.
48. Rappaport D., Furche F.: *J. Chem. Phys.* **2010**, *133*, 134105.
49. Weigend F., Köhn A., Hättig C.: *J. Chem. Phys.* **2002**, *116*, 3175.
50. Reed A. E., Curtiss L. A., Weinhold F.: *Chem. Rev.* **1988**, *88*, 899.
51. Glendening E. D., Badenhoop J. K., Reed A. E., Carpenter J. E., Bohmann J. A., Morales C. M., Weinhold F.: NBO 5.9. Theoretical Chemistry Institute, University of Wisconsin, Madison 2001.
52. MacLeod M. K.: *Ph. D. Thesis*. University of Colorado, Boulder 2011.
53. Peach M. J. G., Benfield P., Helgaker T., Tozer D. J.: *J. Chem. Phys.* **2008**, *128*, 044118.
54. Levine B., Ko C., Quenneville J., Martínez T.: *J. Mol. Phys.* **2006**, *104*, 1039.
55. Reed A. E., Weinhold F.: *J. Am. Chem. Soc.* **1986**, *108*, 3586.
56. Reed A. E., Schleyer P. v. R.: *J. Am. Chem. Soc.* **1990**, *112*, 1434.
57. Weinhold F., West R.: *Organometallics* **2011**, *30*, 5815.
58. Martínez T. J, Ben-Nun M., Levine R. D.: *J. Phys. Chem.* **1996**, *100*, 7884.